ELECTRON BACKSCATTER DIFFRACTION AND PHOTOLUMINESCENCE OF SPUTTERED CdTe THIN FILMS

M. M. Nowell[1,2], M. A Scarpulla[2], A. D. Compaan[3], X. Liu[3,4], N. R. Paudel[3], Dohyoung Kwon[3], and K. A. Wieland[3]
[1]EDAX-TSL, 392 East 12300 South Suite H, Draper UT 84020 USA
[2]Departments of Materials Science & Engineering and Electrical & Computer Engineering, University of Utah, Salt Lake City, UT 84112-9206, USA
[3]Department of Physics and Astronomy, University of Toledo, Toledo, OH 43606, USA
[4]Current address: Institute of Electrical Engineering, Chinese Academy of Sciences, Beijing, 100190, P.R. China

ABSTRACT

Electron backscatter diffraction (EBSD) has been used to characterize the grain size, grain boundary structure, and texture of sputtered CdTe at varying deposition pressures before and after $CdCl_2$ treatment in order to correlate performance with film microstructure. It is known that twin boundaries may have different electrical properties than high-angle grain boundaries and in this work we have included the effects of twin boundaries. We found better correlation of solar cell device performance to the twin-corrected grain size than to the standard grain size. In addition, we have correlated the photoluminescence (PL) spectra with device performance and with the EBSD results. We find that sputtering at 18 mTorr yields the highest efficiency, largest twin-corrected grain size and the strongest PL.

INTRODUCTION

The role that film morphology plays on polycrystalline cadmium telluride (CdTe) thin film solar cells is of major interest [1]. Grain boundaries are expected to act as recombination sites, reducing performance [2]. However grain boundaries are also thought to be able to form a localized electric field, either through structural or impurity effects, which can improve majority and minority carrier separation and improve performance. Enhanced photocurrent has been observed at grain boundaries previously [3, 4]. Grain boundaries can also act as diffusion pathways during the $CdCl_2$ annealing treatment used to produce high-efficiency devices. Grain boundaries could also act as a localized collection site for defects, improving the crystalline quality of the interior of the grains.

Grain boundary density would be expected to influence device performance, and therefore an average grain size could be a useful metric for correlation with device performance. This correlation has been shown in both CdTe [2] and CIGS [5] photovoltaic films. $CdCl_2$ treated films exhibit a large number of twin boundaries, and it is expected that these twin boundaries will exhibit different electrical and diffusional properties relative to random high-angle grain boundaries [6].

To characterize the grain boundary structure and differentiate twin boundaries from random high-angle grain boundaries, Electron Backscatter Diffraction (EBSD) was used to characterize sputtered CdTe films deposited at varying deposition pressures to attempt to correlate measured microstructural features with device performance. EBSD is a technique which allows for the concurrent measurement of the grain size, texture, and grain boundary character distribution of a material [7]. Cell performance and EBSD results were also correlated with photoluminescence spectra of the films grown with similar conditions. These results aid in understanding the active mechanisms of film deposition and growth as well as recrystallization and grain growth accompanying the $CdCl_2$ treatment.

EBSD AND SAMPLE PREPARATION

Sample preparation

The CdTe films were grown on Pilkington TEC glass substrates (TEC7 and TEC15+HRT). The HRT is a proprietary, thin, high resistivity transparent layer. We expect the different substrates do not affect the grain growth. CdS films of 0.11 µm thick were deposited at 18 mTorr. CdTe films were deposited at 5, 18 and 30 mTorr. All CdTe film thicknesses were >2.2 µm with only small variations (~10%) in the final CdTe film thickness, which are not expected to influence device performance[8]. The substrate temperature during deposition was approximately 250 ºC with sputtering under an RF power of 20 W on a 2 inch diameter target. A 30 min 387 ºC $CdCl_2$ treatment was then performed (except for the as-deposited films). After this treatment, 3 nm Cu and 20 nm Au back contacts were evaporated on the performance-characterized films and diffused at 150 ºC for 45 min in air prior to characterization. Prior to both EBSD and device characterization, samples were cut into approximately 5 mm x 10 mm pieces, and samples from the center and edge of the original cells were analyzed to investigate the nonuniformity effects of deposition on device performance and microstructure. Further details on the sputtering procedure and system used are given elsewhere. [9-11]

Experimental details of EBSD

A number of different EBSD preparation techniques for CdTe films have been described previously [12]. However in this work, a different approach termed low-incidence surface-milling (LISM) was used [13]. An FEI Quanta 3D

978-1-4244-9965-6/11/$26.00 ©2011 IEEE

FEG Dual Beam instrument, equipped with both electron and focused Ga+ ion beams (FIB), was used to cut (or mill) a flat analysis plane prior to EBSD. While the 30 kV ion beam energy cuts produced high-quality EBSD patterns from these (and other) CdTe films, it has been previously reported that high-energy FIB milling can affect EBSD pattern quality in semiconducting materials [14, 15], and the authors have observed a strong dependence of EBSD pattern quality with FIB milling energy on some CIGS PV thin films.

Samples were then transferred to an FEI XL-30 FEG SEM to maximize sample throughput. This SEM was equipped with an EDAX-TSL Hikari EBSD detector running OIM Data Collection v5.32. The samples were tilted so that the milled analysis plane was tilted 75º relative to the horizontal (15º relative to the vertical electron beam). Note that the 1.5º incident angle of the FIB cut results in a slight offset of the measured orientation relative to the film surface normal orientation, which was corrected during post data-processing. The EBSD patterns were generated by an electron beam of 20 kV and approximate 3 nA, and collected at a 14 mm working distance. The EBSD detector was set at 100 EBSD patterns per second at a resolution of 96 x 96 pixels and the camera gain set to a value of approximately 5 dB to optimize the signal intensity level. For mapping, EBSD patterns were automatically collected and analyzed at a rate of 100 points/sec from an 18.5 µm x 18.5 µm area using a hexagonal sampling grid with a 25 nm spacing resulting in approximately 640,000 measurements collected in 107 minutes. Prior to map collection, the region of interest was imaged for approximately 30 minutes under the same beam conditions to allow the instrument and sample to stabilize to confirm there is no drifting issues. The mapping location was positioned so that the bottom of the collection area was aligned with the highest portion of the film that was completely smooth after milling and avoiding the transition region between the as-processed surface and the prepared surface.

The collected EBSD mapping data was then analyzed using EDAX-TSL OIM Analysis v5.31. The EBSD indexing rate, which is the percentage of measurement points that are assumed to be analyzed correctly, in this case was determined by the fraction of points with a confidence index (CI) greater than 0.2 after a Grain CI Standardization procedure [16, 17] relative to the total number of points collected. A systematic noise-reduction routine was also applied. Low-confidence points remaining after these steps were excluded from subsequent analysis.

CORRELATION OF EBSD WITH CELL PERFORMANCE

Figure 1 is an image quality map that illustrates the morphology of the center region of the as-deposited CdTe film grown at 30 mTorr. Images from the edge of the growth, approximately 3 cm from this position show slightly smaller grain sizes.

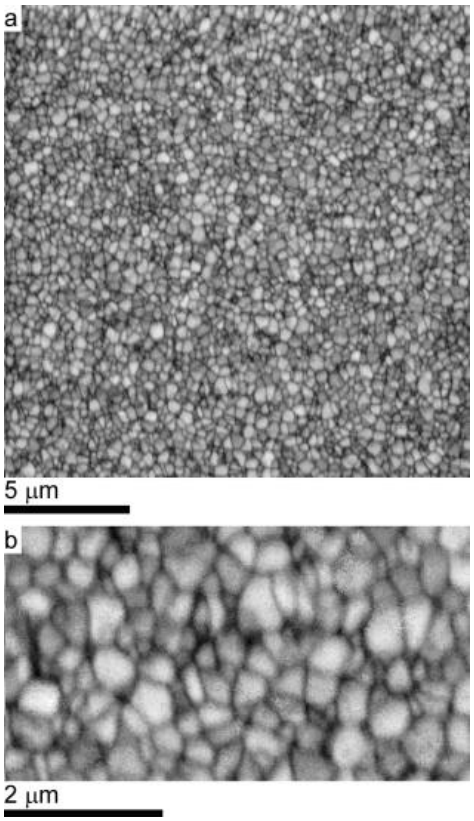

Figure 1 EBSD image quality map from center region of as-deposited 30 mTorr film showing a) full region of interest and b) magnified region of interest.

After activation at 387 ^{o}C there is a large increase in grain size as shown in the EBSD grain maps of Figure 2. Figure 2a includes twin boundaries and Figure 2b excludes twin boundaries so that twinned grains appear as a single grey tone.

These EBSD images were obtained from the center and edge of cell structures grown at 5 mTorr, 18 mTorr, and 30 mTorr yielding twelve distinctly different grain maps. In general the grain sizes remained correlated with the growth conditions even after the extensive grain growth that occurred during the $CdCl_2$ activation treatment. When twin boundaries were included in calculating grain sizes, the cell performance was not well correlated with grain size as seen in Figure 3a. After twin correction (Figure 3b), however, the cell performance exhibits quite strong correlation with the grain sizes as determined from the EBSD images. In this case, the average grain sizes increased in the edge samples from 5 mTorr to 18 mTorr to 30 mTorr, increasing still further in the center region from 5 mTorr to 30 mTorr and then 18 mTorr. It is interesting to note that, although twin-corrected grain size generally increases with increased deposition pressure, the twin-corrected grain size is larger for 18 mTorr than for 30 mTorr. Some of the grain size dependence on sputter

gas pressure may be due to slower film growth as pressure increases. There does appear to be reproducibly a reduced grain size near the edge of the deposition which is also about 10 % thinner than the center. The inversion in grain size between 30 mTorr and 18 mTorr is an interesting test of cell efficiency correlation with twin-corrected grain size. Best cell performance is observed at 18 mTorr which is where the grain size optimizes under the conditions used in this study. However, there are many factors that contribute to cell performance, including ion bombardment effects, substrate temperature, and especially the parameters of the $CdCl_2$ activation treatment, so we do not conclude that twin-corrected grain size is the only or even dominant factor controlling cell performance. It is quite clear that high performance is readily achieved with sub micron grain sizes.

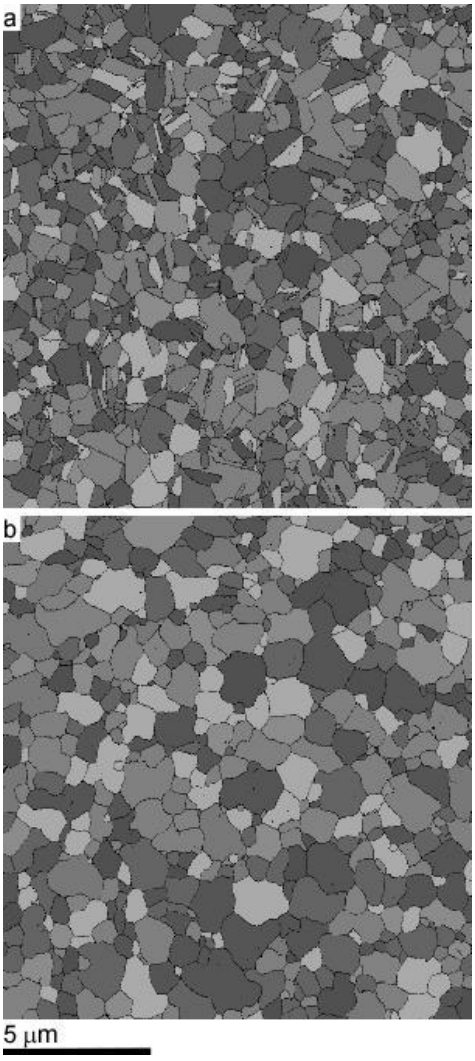

Figure 2 EBSD grain maps a) including and b) excluding twin boundaries for the center region at 18 mTorr after $CdCl_2$ treatment. Grain boundaries are drawn as solid black lines.

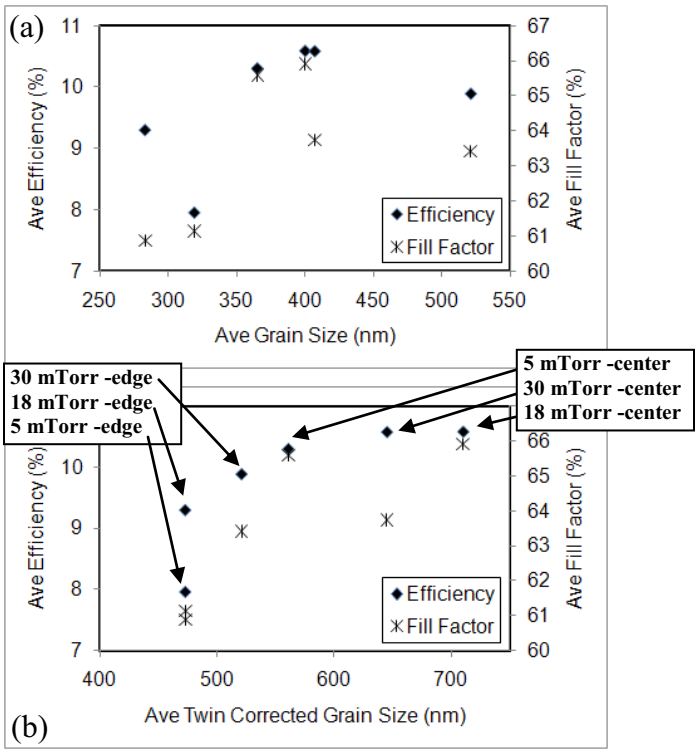

Figure 3 Average efficiency and fill factor versus (a) average grain size and (b) twin-corrected grain size for $CdCl_2$ treated samples.

CORRELATION OF PL WITH CELL PERFORMANCE

Experimental details of PL

The purpose of the photoluminescence (PL) experiments was to determine whether the twin corrected grain size and/or cell efficiency correlate with the PL signatures. The devices for PL experiments were deposited on TEC15+HRT glass under that same conditions used for EBSD devices. CdS films of 0.06 μm thick were deposited at 18 mTorr. CdTe films were deposited at 5, 18 and 30 mTorr and thicknesses were >2.3 μm. RF power and temperature were the same as for EBSD samples. Some cells were given a 30 min 387 ºC $CdCl_2$ treatment similar to that for the EBSD samples. All samples were studied without a back contact (no Cu or Au). PL was taken only from the center piece of each sample. Samples were cut into 6 x 8 mm size and mounted in a He-cooled cryostat. PL was taken from film-side and junction-side at 10 K for both as-deposited and $CdCl_2$ treated films. PL was excited using an argon ion laser operating at 7.5 mW with a wavelength of 514.5 nm. Detection was carried out by a single stage spectrograph (Jobin-Yvon HR640) equipped with a 1024 pixel diode-array InGaAs detector (Princeton Instruments OMA V:1024-1.7). A low photon energy pass filter was used in front of the spectrograph to remove the strong elastically scattered laser light.

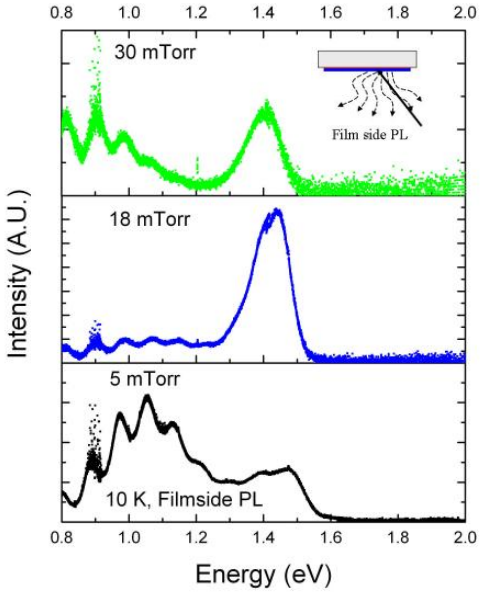

Figure 4 PL of as-deposited CdS/CdTe films observed from film side. (The "noise" near 0.9 eV results from incomplete calibration artifacts due to variable water vapor absorption in the PL beam path.)

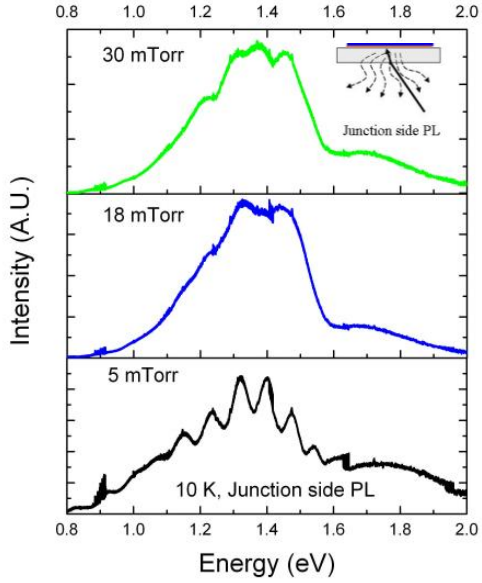

Figure 5 PL of as-deposited CdS/CdTe films observed from junction side.

Results of PL

In Figure 4, as-deposited, film-side PL shows that the 5 mTorr PL has weak near-band-edge PL and a series of deep donor-acceptor pair (DDAP) peaks near 1 eV. A zero-phonon peak at 1.13 eV is followed by several lower-energy vibronic peaks at intervals of about 80 meV. The spectra from the 18 and 30 mTorr samples have a reduced DDAP feature and a much stronger (shallow) donor-acceptor pair (DAP) peaks around 1.4 eV. Note that 18 mTorr, which is the optimum pressure for best cell performance, has the highest ratio of shallow DAP band to DDAP band. Stronger ion bombardment at 5 mTorr may explain the dominant deep defect states of the film.

The as-deposited, junction-side PL in Figure 5, shows little of the DDAP band but a broader DAP band near 1.4 eV. Note that the CdTe is grown on the 0.06 μm CdS layer deposited at 18 mTorr, and the junction-side PL probes this CdS/CdTe region within about 300 nm of the junction. For the 5 mTorr CdTe deposition again there is a strong vibronic series that originates with a zero-phonon peak at 1.479 eV followed by lower energy peaks at about 80 meV intervals.

The 1.479 eV zero phonon peak seen strongly in the junction-side PL involves the A-center acceptor complex V_{Cd}-Cl_{Te} [18] which probably couples strongly to a local vibrational mode that is much higher in frequency than the CdTe bulk phonon of 21 meV. The 1.13 eV zero-phonon DDAP peak is consistent with the peak discussed by Krustok, et al. [18] that they attribute to a V_{Te} coupled to a Te interstitial. Again, it apparently has very strong phonon coupling. We speculate, based on cell performance (see below) that strong DDAP features are disadvantageous to good cell performance.

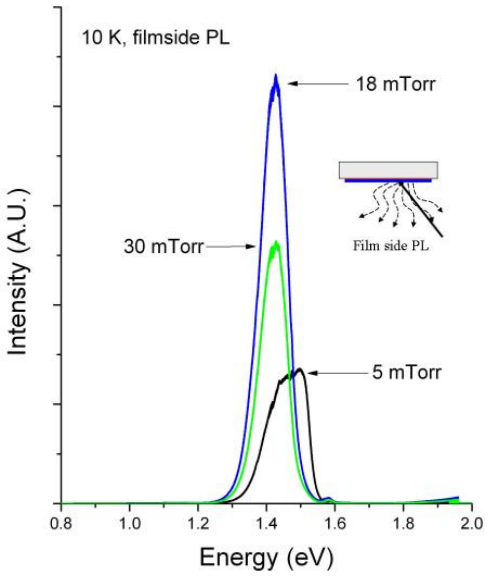

Figure 6 PL of $CdCl_2$ treated films observed from CdTe film side.

In Figure 6, showing film-side PL after $CdCl_2$ treatment, the intensity increases 3 or 4 orders of magnitude and all vibronic features are suppressed. The much stronger PL

intensity of the 1.424 eV band compared with the as-deposited films, indicates that nonradiative transitions are greatly suppressed, consistent with many fewer recombination centers than in as-deposited films. Also near 1.59 eV, a weak bound exciton peak appears after $CdCl_2$ treatment, which is an indicator of improved crystallinity and minority carrier lifetime.

In spite of the activation, it seems that deposition pressure information is carried on after $CdCl_2$ treatment. For example, the 18 mTorr sample, which has the highest ratio of shallow to deep defect PL intensity before $CdCl_2$ treatment, also shows the strongest PL after treatment. After treatment, the PL of the 30 mTorr sample looks similar to the 18 mTorr sample, except slightly less intensity. The 5 mTorr sample PL, which we suspected as having ion damage, has a much broader peak and lower intensity, implying relatively more nonradiative transitions due to defects.

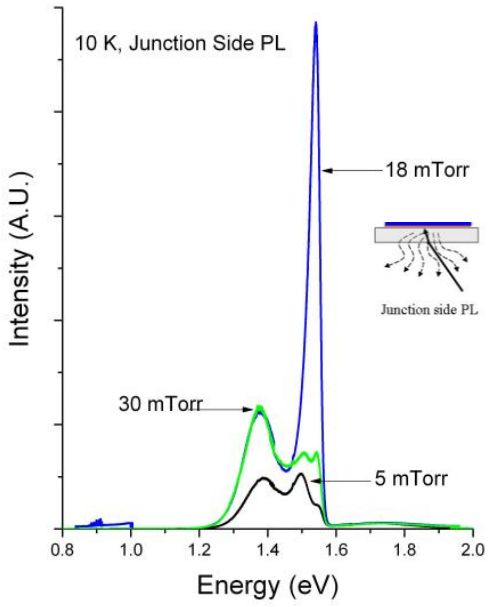

Figure 7 PL of $CdCl_2$ treated CdS/CdTe films observed from junction side.

Figure 7 shows junction-side PL of $CdCl_2$ treated films. We consistently find that the 18 mTorr film has a stronger and narrower PL peak at 1.541 eV than either the 30 mTorr or 5 mTorr samples. All have a peak at 1.377 eV in junction side PL which is probably related to the S alloying in CdTe near the junction. The 18 mTorr and 30 mTorr samples have similar peaks but at 1.424 eV in $CdCl_2$ treated film-side PL. The energy difference, 47 meV, can be attributed to the intermixing of CdS_x and $CdTe_{(1-x)}$, in this case x=0.062.[19] Thus, we know that CdS and CdTe composition of 18 mTorr and 30 mTorr are close. We also know from as-deposited films' PL (Figure 4, 5) 18 mTorr and 30 mTorr are similar. That similarity appears to be consistent with the fact that 18 mTorr and 30 mTorr films have similar average grain size (~400 nm) without twin correction in Figure 3 (a).

CONCLUSIONS

We have investigated the effects of the sputtering process (chiefly pressure) on the resulting CdTe film microstructure using EBSD data, on recombination processes using PL data, and on cell performance using cell efficiency and fill factor data. If twin boundaries are excluded from the grain size calculation (twin correction), the center of the 18 mTorr film has the largest average grain size (710 nm) after $CdCl_2$ treatment followed by the 30 mTorr and 5 mTorr samples, respectively. A positive correlation was established between the EBSD twin-corrected grain size and the cell performance parameters across all sputtering pressures and locations on the samples (center vs. edge). The center of the 18 mTorr film has the strongest near-band-edge PL at 1.5 eV followed by the 30 mTorr and 5 mTorr samples, respectively indicating that the density of non-radiative defects is negatively correlated with the twin-corrected grain size. The data for films deposited at 5 mTorr showed smaller grain sizes and PL spectra suggestive of ion damage that carries through the $CdCl_2$ activation process.

In summary, both the details of defect states as measured with PL on $CdCl_2$-treated CdTe films sputtered at different pressures as well as the cell efficiency and fill factor of completed devices made from the same films are correlated with twin-corrected grain size as determined using EBSD. Aspects of the PL data are consistent with the findings of EBSD that films with larger twin-corrected grain sizes have fewer non-radiative recombination centers and yield cells having better performance. The correlations between EBSD twin-corrected grain sizes, near-band-edge PL intensity and cell performance data and lack of good correlations with the *non-twin-corrected* grain sizes suggests that twin boundaries exhibit much lower non-radiative recombination than do general grain boundaries. Further details of this work can be found in Ref. 20.

ACKNOWLEDGEMENTS

This work is supported by the U.S. DOE University Photovoltaic Process and Product Development program.
.

REFERENCES

[1] I. Visoly-Fisher et al., "How Polycrystalline Devices Can Outperform Single-Crystal Ones: Thin Film CdTe/CdS Solar Cells", *Adv. Mater.* **16**, 2004, pp. 879-883.

[2] J.D. Major et al., “Control of Grain Size in Sublimation-Grown CdTe, and the Improvement in Performance of Devices with Systematically Increased Grain Size,” *Sol. Energy Mater. & Sol. Cells* **94**, 2010, pp. 1107-1112.

[3] I. Visoly-Fisher et al., “Understanding the Beneficial Role of Grain Boundaries in Polycrystalline Solar Cells from Single-Grain-Boundary Scanning Probe Microscopy,” *Adv. Funct. Mater.* **16**, 2006, pp. 649 - 660.

[4] I. Visoly-Fisher, S.R. Cohen, and D. Cahen, “Direct Evidence for Grain-boundary Depletion in Polycrystalline CdTe from Nanoscale-resolved Measurements,” *Appl. Phys. Lett*. **82**, 2003, pp. 556-558.

[5] T. Eisenbarth et al., “Origin of Defects in $CuIn_{1-x}Ga_xSe_2$ Solar Cells with Varied Ga Content”, *Thin Solid Films* **517**, 2009, pp. 2244-2247.

[6] D. Abou-Ras et al., “Grain-boundary Types in Chalcopyrite-type Thin Films and Their Correlations with Film Texture and Electrical Properties”, *Thin Solid Films* **517**, 2009, pp. 2545-2549.

[7] R.A. Schwarzer, D.P. Field, B.L. Adams, M. Kumar, A.J. Schwartz, in: A.J. Schwartz, M. Kumar, D.P. Field, B.L. Adams (Eds.), *Electron Backscatter Diffraction in Materials Science*, 2nd Edition, New York: Springer, 2009, pp. 1.

[8] V.V. Plotnikov et al., “Magnetron Sputtering for II-VI Solar Cells: Thinning the CdTe”, *Mater. Res. Soc. Symp. Proc.* **1165**, 2009, pp. M09-01.

[9] M. Shao et al., “Radio-frequency-magnetron-sputtered CdS/CdTe Solar Cells on Soda-lime Glass,” *Appl. Phys. Lett*. **69**, 1996, pp. 3045-3047.

[10] A. Gupta, V. Parikh and A. Compaan, “High Efficiency Ultra-thin Sputtered CdTe Solar Cells”, *Sol. Energy Mater. & Sol. Cells* **90**, 2006, pp. 2263–2271.

[11] A.D. Compaan, “Photovoltaics: Clean Power for the 21st Century”, *Sol. Energy Mater. & Sol. Cells* **90**, 2006, pp. 2170-2180.

[12] H.R. Moutinho et al., “Electron Backscatter Diffraction of CdTe Thin Films: Effects of $CdCl_2$ Treatment”, *Journal of Vacuum Science & Technology. A: International Journal Devoted to Vacuum, Surfaces, and Films* **26**, 2008, pp. 1068-1073.

[13] S. Zaefferer, S.I. Wright and D. Raabe, “Three-Dimensional Orientation Microscopy in a Focused Ion Beam–Scanning Electron Microscope: A New Dimension of Microstructure Characterization**”,** *Metall. Mat. Trans. A* **39**, 2008, pp. 374-389.

[14] J.R. Michael and L.A. Giannuzzi, “Improved EBSD Sample Preparation Via Low Energy Ga+ FIB Ion Milling” *Microsc. Microanal*. **13**, 2007, pp. 926-927.

[15] T.L. Matteson et al., “EBSP Investigation of Focused Ion Beam Surfaces”, *Journal of Electronic Materials* **31**, 2002, pp. 33-39.

[16] D.P. Field, “Recent Advances in the Application of Orientation Imaging,” *Ultramicroscopy* **67**, 1997, pp. 1-9.

[17] M.M. Nowell and S.I. Wright, “Orientation Effects on Indexing of Electron Backscatter Diffraction Patterns”, *Ultramicroscopy* **103**, 2005, pp. 41-58.

[18] See for example; X. Liu and A. D. Compaan, “Photoluminescence from Ion Implanted CdTe Crystals” *Mater. Res. Soc. Symp. Proc.* **865**, 2005, pp. F5.25 and J. Krustok et al., “Deep Centre Luminescence in P-type CdTe”, *J. Appl. Phys*. **80**, 1996, pp. 1757-1762.

[19] A. Luque and S. Hegedus, *Handbook of Photovoltaic Science and Engineering*, John Wiley& Sons, 2003, pp. 637-641.

[20] M.M. Nowell et al., “Characterization of Sputtered CdTe Thin Films with Electron Backscatter Diffraction and Correlation with Electrical Performance”, *submitted to Thin Solid Films.*